Proceedings of the 7th International Conference on Civil Structural and Transportation Engineering (ICCSTE'22)
Niagara Falls, Canada – June 05-07, 2022
Paper No. 214
DOI: 10.11159/iccste22.214

Structure Health Monitoring Of Concrete Structures Using Magnetic Flux Leakage

Yihan Zhang[1], Qing Wang[2], Songling Huang[2]
[1]Department of Engineering, Durham University
DH1 3LE, United Kingdom
Yihan.zhang@durham.ac.uk; qing.wang@durham.ac.uk
[2]Department of Electrical Engineering, Tsinghua University
Beijing, 100084, China
huangsling@tsinghua.edu.cn

Abstract **-** Reinforcing bar, usually made of steel, is widely used in civil structures to increase the tensile strength of concrete. Heat-induced delayed expansion and corrosion expansion resulting in rust occupies a greater volume than rebar. This expansion creates tensile stress in the concrete which can eventually cause cracking, delamination and spalling. Non-destructive testing (NDT) is a testing technology that detects the presence of defects in the material or detects the physical or mechanical properties of the material without destroying the material. In this paper, the emergence, development and application of magnetic flux leakage testing technology are presented. The principle and working process of three-valved open electromagnetic coil magnetic flux leakage detection devices is used for rebar defect detection, as well as introducing the design method of its main components. The three-valved open electromagnetic coil magnetic flux leakage detection method is optimized through simulating the variation of magnetic flux density and detection defects between different magnetizer radii. The test results show that compared to other detection methods the three-valved magnetizer has the ability to detect rebar defects with high precision, and as the radius of the magnetizer increases, the magnetization of the steel bars in the central magnetizer area of the magnetizer gradually attenuates, and the amplitude of the detection signal also decreases, showing the characteristic of slow decay.

Keywords**:** Structural health monitoring, open electromagnetic coils, tubular coils, concrete rebar, magnetizer, magnetic flux leakage.

1. Introduction

Rebar is one of the most crucial elements in concrete structures as it directly determines the performance of compression, shear, and seismic and shock resistance of the structure, and affects its safety and durability [1]. The location, diameter, cover thickness and fracture location of rebar are important factors to ensure effective detection and evaluation of durability [2]. Miyagawa and Seto [3] researched and analyzed the brittle fracture of concrete steel bars, as shown in Figure 1. Reliable evaluation and prediction results can be obtained depending on reliable testing data. Jiles [4] pointed out that the NDT of concrete structural rebar is to determine physical quantities concerning its structural quality using physical methods such as sound, light, electricity, magnetism, heat and rays without affecting its performance. This is achieved by testing and through the correlation analysis between the measured physical quantity and its structural strength, size and integrity. In a study conducted by Regor [5], NDT was classified into six categories and more than 70 variations, such as ultrasonic testing, X-ray testing, magnetic particle testing, penetration testing, radar monitoring, and some unusual ones like acoustic emission, leak testing, holographic lithography, photography, infrared thermography and microwave testing, which are common in practical applications.

Fig. 1: Example of fractured steel bar.

2. Magnetic flux leakage technology

Magnetic flux leakage is a non-destructive testing method based on magnetic particle testing technology, which uses magnetic phenomena to detect the surface and near-surface defects of ferromagnetic components.[6] The basic principle is that ferromagnetic materials are magnetized under the action of an external magnetic field, as shown in Figure 2. If there are no defects in the material, most of the magnetic lines of force pass through the ferromagnetic materials and evenly distribute inside the material[7]. If the surface or near surface of this material has cracks or other defects, the magnetic field passing through the area will be distorted and the magnetic lines will be bent, and partial magnetic lines will leak out of the surface to form a leakage magnetic field due to the fact that the magnetic permeability of the defect in the ferromagnetic material is much larger than the magnetic resistance of the small defect itself [8]. Defective leakage magnetic fields are detected by magnetic sensitive elements to generate electrical signals, and the defect conditions can be found by processing the signals.

Traditional non-destructive testing devices use magnets as iron cores when measuring the structure. Due to the sensor device being attached to the iron core and magnet, the magnets will attract each other and so will not be able to carry out axial sliding scanning and will cause damage to the sensor. Therefore, pure iron is used as the core. An electric current is generated, and a magnetic field is generated by wires of copper wire wound around the core.

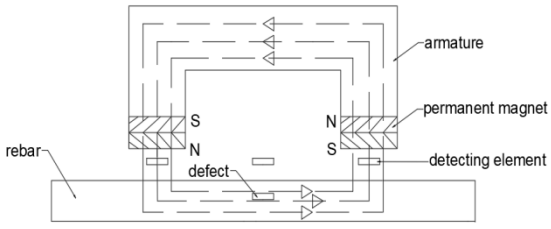

Fig. 2: Schematic diagram of traditional magnetic principle.

3. Theory

The open coil has the additional advantage of dividing each magnet coil into a closed loop current. The vertical and inward magnetic field generated inside the coil of a semicircular line current is indicated in Figure 1. A circuit must be constructed for current according to charge conservation [11]. Therefore, a three-valved open electromagnetic coil can be used to construct two line currents in opposite directions. The magnetic fields generated by these two currents are also in opposite directions while overlapping. It can be known from the Biot-Savart Law [12] that:

$$\mathbf{B} = \frac{\mu}{4\pi}\int \frac{Id\mathbf{l}\times\mathbf{r}}{r^3} \tag{1}$$

where B is the magnetic field, μ is the magnetic conductivity, I is the amount of line current, dl is the micro unit of a line current path with a direction, and r is the displacement vector between dot and line.

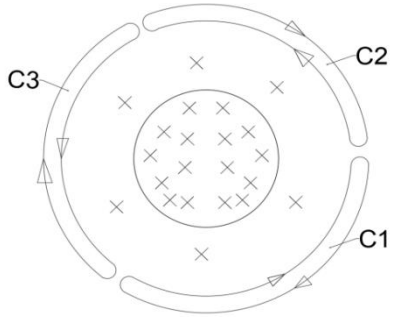

Fig. 3: The current element of the coil. C1, C2, C3 is path of current.

As shown in Figure 3, when the distance between the dot and the current element of the coil is much greater than that between the three semicircular coils, we approximately assume that:

$$\frac{\mu}{4\pi}\int_{l_1} \frac{Id\mathbf{l}\times\mathbf{r}}{r^3} = \frac{\mu}{4\pi}\int_{l_2} \frac{Id\mathbf{l}\times\mathbf{r}}{r^3} = \frac{\mu}{4\pi}\int_{l_3} \frac{Id\mathbf{l}\times\mathbf{r}}{r^3} = 0\Big|_{l_1=l_2=l_3=0} \tag{2}$$

Where I1, I2 and I3 is the current distributed through C1, C2 and C3.

As the currents of the three coils are in opposite directions, we also assume that the radii of these three coils are approximately equal, so the results of these three semicircular integrals are equal while the symbols are opposite.

$$\frac{\mu}{4\pi}\int_{C_1} \frac{Id\mathbf{l}\times\mathbf{r}}{r^3} + \frac{\mu}{4\pi}\int_{C_2} \frac{Id\mathbf{l}\times\mathbf{r}}{r^3} + \frac{\mu}{4\pi}\int_{C_3} \frac{Id\mathbf{l}\times\mathbf{r}}{r^3} = 0 \tag{3}$$

4. Three-dimensional finite element simulations

According to the above principal formula, the magnetic field, which is generated by the reverse current of the external coil bias, is generated by the forward current. In order to eliminate the effect of the current on the external coil, an iron core is added between the three coils. The magnetism generated by the external coil is passed through the Ferrous core, an open detection device that can be constructed with three C-shaped coils with a black iron core, detail dimension in Figure 4.

It should be noted that the current direction of the three C coils ensures that a loop direction can be formed in the three internal coils, so that the distribution of the magnetic field generated is consistent with the distribution of the closed coil. Different-sized radii of the iron core are adopted, as shown in Table 1. Simulation is conducted according to different-sized radii, as shown in Figure 5.

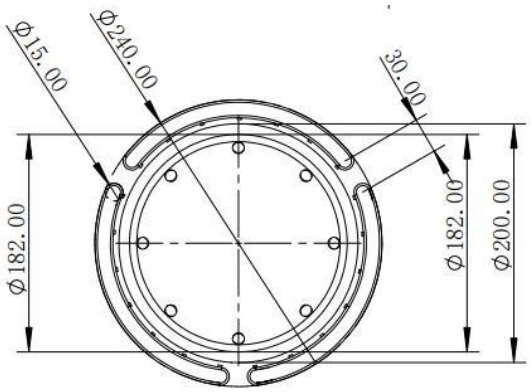

Fig. 4: Schematic diagram of coil and concrete structure.

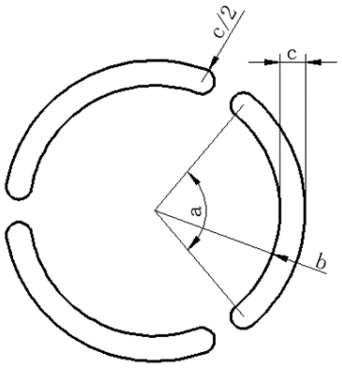

Fig.5. Magnetizer radius design.

Table 1: Caption for table goes at the top.

Magnetizer radius / **Core size (/mm)**	102	104	106	108	110	112
Three-valved core Angle (a)	98	98.2	98.4	98.6	98.8	99
Core diameter (b)	114	116	118	120	122	124
The thickness of the core (c)	15	15	15	15	15	15
The axial length (d)	120	120	120	120	120	120

ANSYS software is used to simulate the magnetic flux leakage testing device. The finite element model has been created as shown in Figure 6. The size of the model is a concrete cylindrical structure with a diameter of 200mm and a length of 15000mm. The longitudinal bars are eight rebar steels with a diameter of 10mm and stirrups with a diameter of 6mm and a spacing of 200mm to form concrete members and the use of concrete C25 type. The magnetizer input current with a density of $1 * 10^7 \mathrm{A}/m^2$ and a copper wire with a thickness of 12mm for winding. The defect size is set at 8mm. The signal is taken along the exterior surface of the cement towards the position, 95mm from the radial direction. X, Y and Z represent the radial, circumferential and axial directions in the cylindrical coordinate system, respectively. This can be seen in Figure 6.

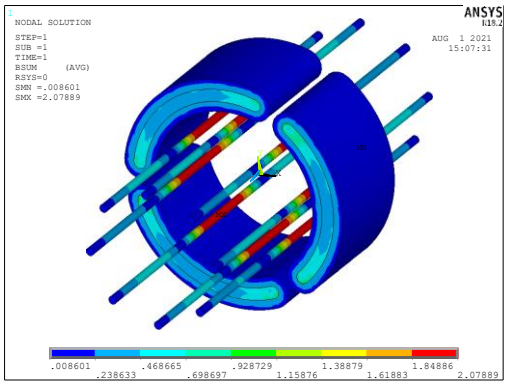

Fig. 6: Overall magnetization 3D magnetization cloud map.

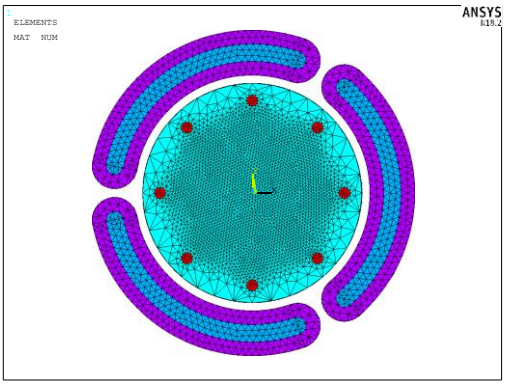

Fig. 7: The simulation model of the electromagnetic coil using ANSYS.

Analysis of the meshing results in Figure 7 show that the size of rebar and hoop is smaller than that of the surrounding concrete and magnetizer, therefore it is necessary to take into account the large size and rough mesh of concrete and magnetizer to reduce the computational burden in the process of meshing. At the same time, the rebar to be detected is refined to accurately extract the magnetic flux density signal. The local meshing around the reinforcement and defects is shown in Figure 8 and the results are described in section V.

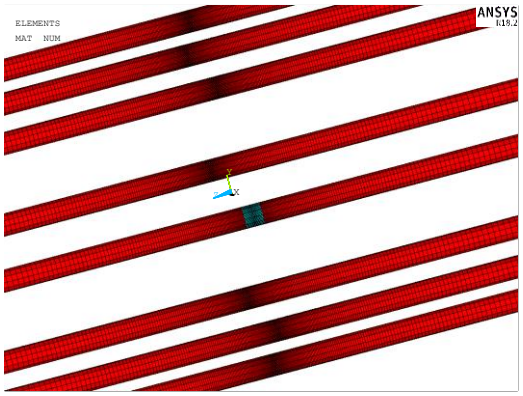

Fig. 8: Local meshing showing the distribution of the defects.

5. Results

Figure 9 shows the size of the magnetic flux density generated by magnetizers with different radii on Bx with and without defects：

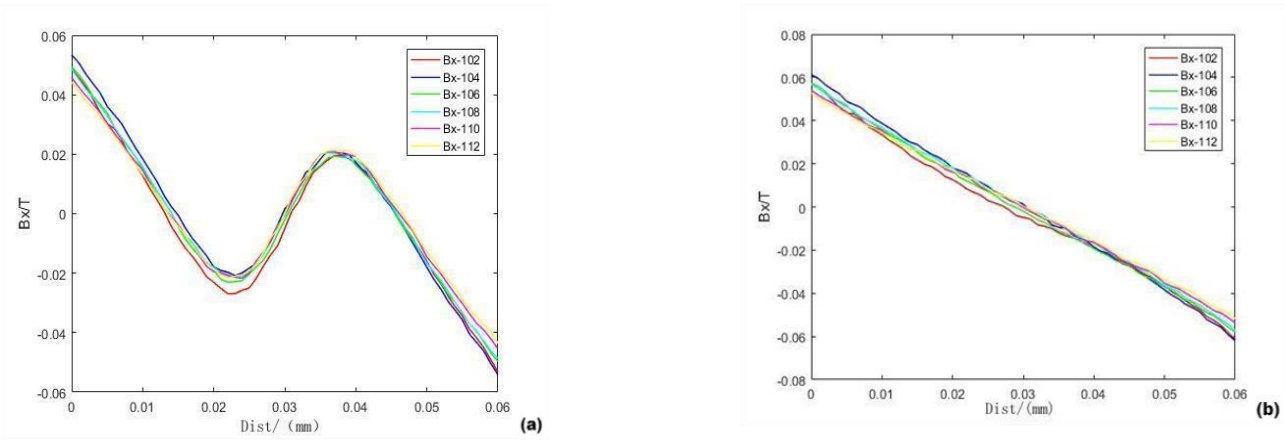

Fig. 9: The magnitude of magnetic flux density generated in the X directions.

As shown in Figure 9(a) and (b) above, it is observed by the magnetic flux density calculations of rebar with defects using magnetizers of different radii that the Bx signal presents the characteristics of the wave crest and trough successively in the radial extraction path near the defect, which suggests that the magnetic flux density of the defect gradually changes from magnetic hole area to reinforcement area, then the magnetic flux shows a jumping fluctuation.

Figure 10 shows the size of the magnetic flux density generated by magnetizers with different radii on By with and without defects :

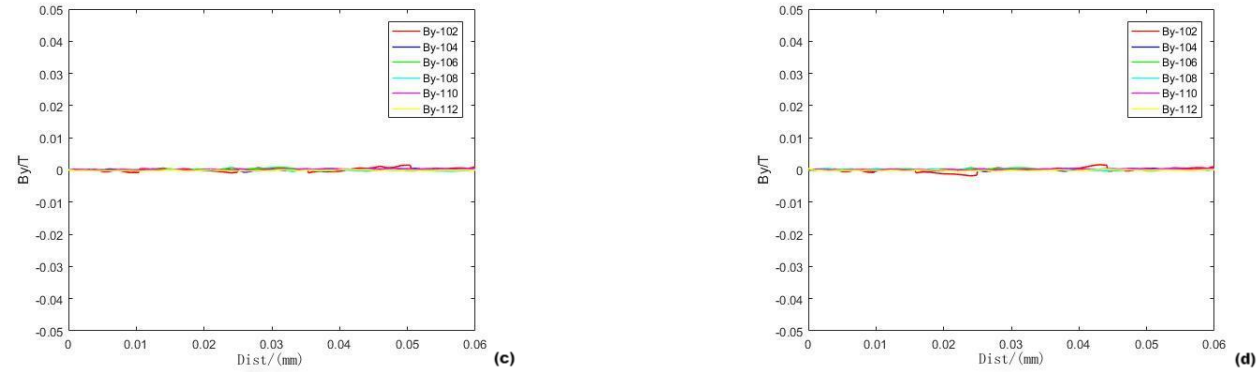

Fig. 10: The magnitude of magnetic flux density generated in the Y directions.

As shown in Figure 10(c) and (d), the calculation results of the magnetic flux density under different magnetizer radii when the rebar presented in the above figure is without defects shows that the calculated By on the circumferential path almost appears as a straight line, which indicates that the rebar and concrete presents circumferential uniform magnetization under the circumferential clasping magnetization of the three-valve magnetizer. And because the steel bar defects are disconnected, the circumferential magnetic field does not change significantly when there are defects.

Figure 11 shows the size of the magnetic flux density generated by magnetizers with different radii on By with and without defects:

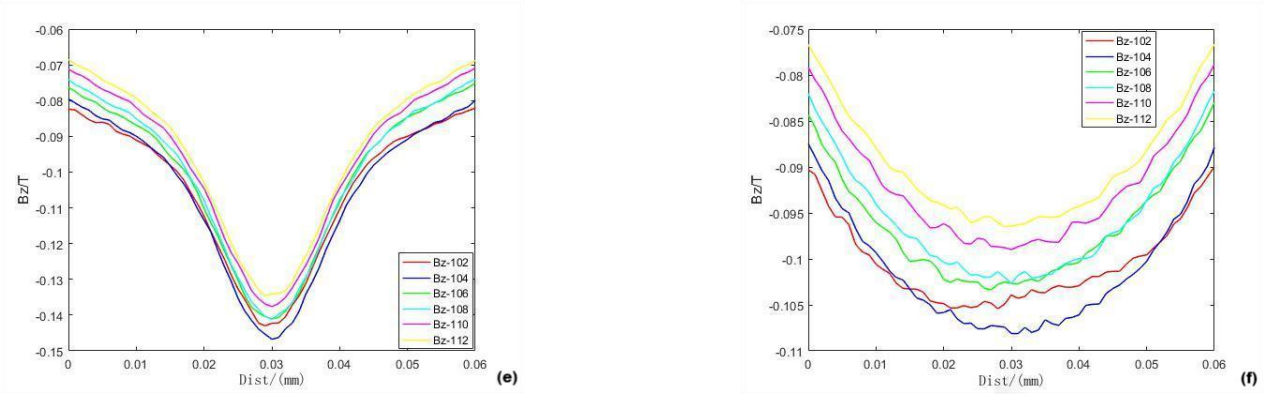

Fig. 11: The magnitude of magnetic flux density generated in the Z directions.

As shown in Figure 11(e) and (f), the axial Bz calculation shows that the rebar has the maximum magnetic flux leakage directly above the defect, so the extracted signal presents the intermediate trough maximization, and the magnetization intensity of the rebar and the amplitude of the detection signal in the central magnetizer decreases gradually as the radius of the magnetizer increases. According to the calculation results of axial Bz when there is no defect, the flux density presents a big wave trough, and the amplitude of the detection signal attenuates slowly with the increasing radius of the magnetizer, which attributes to a strong reverse magnetic background field in the axial central region and a weak field near both sides of the magnetizer.

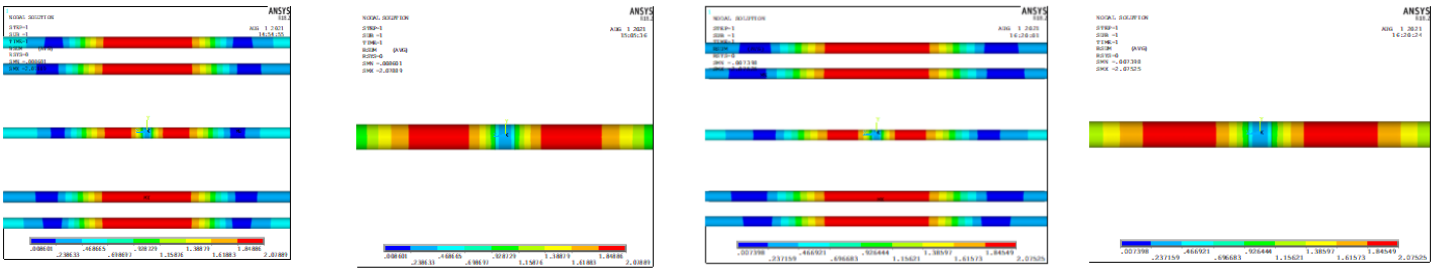

Magnetic nephogram results at 102mm magnetizer radius. Magnetic nephogram results at 108mm magnetizer radius.

Fig. 12: The magnetic field cloud map.

Because the simulation results show that the laws of the magnetic cloud images under different magnetizer radii are consistent, Figure 12 only shows the magnetic cloud images under part of the radius. It can be observed in the magnetic simulation nephogram of different magnetizers that the middle region of the rebar sample has a higher magnetization corresponding to the inside of the magnetizer and presents a red area in a certain axial direction. The magnetic flux density on both sides of the magnetizer away from the central magnetization area is relatively weak, and as the radius of the magnetizer changes or gradually increases, the axial magnetization field distribution of the magnetic flux density in the central area is consistent, that is, it shows a high magnetic flux intensity in the middle section of the magnetizer but is weak on both sides, and the observation of the rebar sample with defects shows that only the magnetic background field in the air domain appears because of broken rebar at the defect. Therefore, the magnetic flux density at the defect presents a sudden drop, which is consistent with the trough signal in the magnetic flux density detection signal, indicating consistent simulation results.

6. Conclusion

This research introduces the idea and its application analysis in the electromagnetic field. The tasks accomplished are as follows: 1). A defect detection device model for rebar in concrete structures was established using the finite element

software, and the magnetic flux leakage field distribution, and radial and axial magnetic flux leakage nephogram were obtained. 2). The characteristics of radial and axial magnetic flux leakage signal waveforms were analyzed. 3). The related axial and radial component waveforms of the leakage magnetic field were obtained by changing the radius of the magnetizer from 102mm to 112mm, and the influence and law of the geometric parameters of different magnetizers on the defect magnetic flux leakage signal were studied. The results show that the smaller the radius of the magnetizer, the more accurately the defect can be detected.

References

[1] Yin X, Hutchins DA, Diamond GG, Purnell P. Non-destructive evaluation of concrete using a capacitive imaging technique: preliminary modelling and experiments. Cement Concrete Res; 2010, 40: 1734–1743.

[2] Maierhofer, C. ArSHM R. and Rollig, M. Application of impulse-thermography for non-destructive assessment of concrete structures. Cement Concrete Comp, 2006, 28, pp. 393–401.

[3] Miyagawa, T., Seto, K., & Sasaki, K. Fracture of Reinforcing Steels in Concrete Structures Damaged by Alkali-Silica Reaction. Advanced Concrete Techology, 2006, 4, pp.339–355.

[4] D. C. Jiles, Review of magnetic methods for nondestructive evaluation (part 2), NDT International, Vol 23. No 2. April 1990, P83.

[5] Regor S, Nathanael G, Ken C, Eric M. Nondestructive Methods and Special Test Instrumentation Supporting NASA Composite Overwrapped Pressure Vessel Assessments [C]. 48th AIAA/ASME/ASCE/AHS/ASC Structures, Structural Dynamics, and Materials Conference, Honolulu, Hawaii. Apr. 23-26, 2007: 1-18.

[6] Newswire, P. Global Non-Destructive Testing (NDT) Equipment Market - By Technology (Ultrasonic, Eddy Current, Electromagnetic, Radiography, Thermography), Verticals (Manufacturing, Petrochemical, Aerospace, Automotive, Power Generation) & Geography (2013 - 2018), PR Newswire.

[7] Usamentiaga, R., Venegas, P., Guerediaga, J., Vega, L., & López, I. Automatic detection of impact damage in carbon fiber composites using active thermography. Infrared Physics & Technology, 2013, 58(0), 36-46.

[8] Maierhofer, C., Myrach, P., Reischel, M., Steinfurth, H., Röllig, M., & Kunert, M. Characterizing damage in CFRP structures using flash thermography in reflection and transmission configurations. Composites Part B: Engineering, 2014, 57(0), 35-46.

[9] Sun, Y. and Kang, Y. A new MFL principle and method based on near-zero background magnetic field. NDT&EInt, 2010, 43, pp. 348–35.

[10] Sharatchandra, Singh. W., Rao, B.P.C., Thirunavukkarasu, S. Flexible GMR sensor array for magnetic flux leak-age testing of steel track ropes. J Sensor 2012; 129074, pp. 1–6.

[11] Islam S.M, Khalil, Anke Klingner, Sarthak Misra. Mathematical Modeling of Swimming Soft Microrobots, Chapter 3 - Theory of electromagnetics: Soft-magnetic bodies, 2021, pp.43-59.

[12] A.L.Stanford, J.M.Tanner. Physics for Students of Science and Engineering. Magnetic Fields I, 2014, pp. 452-483.